Supplementary Information (SI) for Nanoscale.
This journal is © The Royal Society of Chemistry 2025

Supplementary information (SI)

Unveiling the Transformation of CoNi Hydroxides to CoNiFe Layered Double Hydroxides with an Implications of Electron Modulation in One step Coprecipitation for Efficient Oxygen Evolution Electrocatalysis†

Jony Saha* and Firdosh Alam Molla

Department of Applied Chemistry, Maulana Abul Kalam Azad University of Technology
West Bengal-741249

Email: jonysaha85@gmail.com

Chemical

Nickel nitrate hexahydrate (Ni $(NO_3)_2.6H_2O$), cobalt chloride hexahydrate ($CoCl_2.\ 6H_2O$), ferric chloride ($FeCl_3$) and nafion perfluronated resin solution were purchased from Sigma- Aldrich Pvt.Ltd. Sodium hydroxides (NaOH), sodium carbonate (Na_2CO_3), potassium bromide (KBr) and potassium hydroxide (KOH) were supplied by Avra Synthesis Pvt. Ltd. Nitric acid (HNO_3), ethanol and isopropanol were bought from Merck Chemicals Pvt. Ltd. Double distilled water was used throughout the study.

Experiments:

Synthesis of CoNiFeLDH:

In the synthesis of CoNiFeLDH, two sets of solution were prepared. Firstly, the Set -A solution was prepared with 0.70 gm of NaOH and 0.60 gm of Na_2CO_3 in 10 ml of double distilled water. The synthesis of Set B solution was prepared by dissolving 0.60 gm of Ni $(NO_3)_2.6H_2O$, 1.5 gm of $CoCl_2.\ 6H_2O$ and 1.0 gm of $FeCl_3$ in 10 ml double distilled water. Then, the Set-A and Set-B solutions were added dropwise to 20 ml double distilled water and stirred the solution at pH=9 for 24 h. Afterward, the filtration was carried out and the precipitate was washed with water and ethanol. Then the filtered residue was dried in hot air oven for 12h at 50 º C.

Synthesis of CoNi hydroxide:

In the synthesis, 0.70 gm of of NaOH and 0.60 gm of Na_2CO_3 were added to 10 ml of double distilled water, labelled as Set-A. Then another set of solutions was prepared, namely Set-B. In Set B, 0.60 gm of Ni $(NO_3)_2.6H_2O$ and 1.5 gm of $CoCl_2.\ 6H_2O$ were dissolved in 10 ml double distilled water. Afterwards both the set of solutions were added dropwise to 20 ml of double distilled water in stirring condition at pH=9 for 24 h. The precipitation obtained from the solution was filtered off and washed with water and ethanol. Finally, the filtered residue was dried in hot air at 50 º C for 12h.

Characterisation:

Fourier transform infra-red (FTIR) spectra of CoNi hydroxide and CoNiFeLDH was carried out using Shimadzu FTIR spectrometer. To analyse, samples were grinded with KBr to make a pellet and recorded the spectra in 4000 -400 cm^{-1} range with a resolution of 4 cm^{-1} in transmission mode. X-ray diffraction of the materials was analysed with Brukar D8 Advance diffractometer by Cu Kα radiation of wavelength of 1.5405Å operating 45 kV and 200 mA. The Raman spectra were performed on a Confocal Photoluminescence Raman Spectro microscope (Model: WITec Alpha 300 R) under an excitation of 532 nm laser light with the power of 0.20 mW. For quantitative analysis, an inductively coupled plasma optical emission spectroscopy (ICP-OES) with Perkin Elmer -Avio 200 was used to estimate the number of moles of Ni, Co and Fe in the respective samples. In the analysis, a known amount of CoNiLDH and CoNiFeLDH was heat-treated separately and transfer the residue in two different beakers to dissolve in

10% HNO_3 solution for ICP-OES analysis in Perkin Elmer Avio 200. N_2 adsorption desorption isotherm was carried out at -196 ^{O}C before degassing the samples at 120 ^{O}C for 4h under a vacuum of 10^{-2} Quantachrome NovaWin surface area and pore size analyser. A multipoint Brunauer -Emmett-Teller (BET) and Barrett -Joyner -Helenda method were followed to estimate pore size distribution and surface area of the samples. For TEM studies, powder samples were dispersed in ethanol and placed one drop on the carbon coated Cu grid to record image and elemental analysis using JEOL-JEM F200 electron microscope with an accelerating voltage of 200 kV. X-ray photoelectron spectroscopy (XPS) of the samples was carried out using Thermofisher Nexsa with an Al Kα X-ray monochromatic source (hν =1486.6 eV). Zero field cooling Temperature (ZFC-T) dependent magnetic susceptibility was carried out in 10-300 K using DynaCool (Model: PM-S9).

Electrochemical analysis:

The oxygen evolution reaction with the characterised materials was carried out using electrochemical workstation, Kanopy Tech (Model: PGLyte 1.0). In the experiment three electrodes configuration was used using reference electrode of Ag/AgCl in saturated KCl solution, Pt wire as a counter electrode and glassy carbon as working electrode (electrode diameter = 3 mm area, 0.07 cm^2). Prior to the electrochemical analysis, the synthesised materials were deposited as catalyst ink on glassy carbon electrodes to make it working electrode for the electrochemical cell. Accordingly, the catalyst ink was prepared by mixing 1.2 mg of the sample, 250 µL of distilled water-isopropanol (v/v=3:1) and 12.5 µL of nafion perfluorinated resin solution followed by sonication for 5 min to make well disperse ink. In the next step, glassy carbon electrode was polished with the alumina powder of 0.3-micron particle size, and 1 µL of the catalyst ink was deposited on the polished surface of glassy carbon. The glassy carbon electrode was dried at 50 °C for 30 min to set up in electrochemical cell with the Ag/AgCl reference electrode and Pt wire counter electrode in 1M KOH electrolyte solution. Linear sweep voltammogram (LSV) was recorded from 0 to 1 V region at 2mV/sec scan rate with respect to Ag/AgCl potential. The potential obtained with respect to Ag/AgCl electrode was converted to reversible hydrogen electrode (RHE) following, E (RHE)= E(Ag/AgCl) + 0.196 + 0.059 pH, considering the contribution pH of the electrolyte solution in the electrochemical analysis. The data obtained in the electrochemical analysis was reported without IR drop correction throughout the study. A constant current electrolysis (Chronopotentiometry) was performed at 10 mA cm^{-2} for 12 h. Electrochemical impedance spectroscopy (EIS) was carried with l amplitude of 0.005 V in a frequency range of 10^5 to 10^2 Hz. Mass activity, specific activity, turnover frequency (TOF) of the catalysts were calculated following Eqs. S1, S2 and S3, respectively.[1,2]

$$\text{Mass activity} = \frac{j}{m} \quad \text{(S1)}$$

$$\text{Specific activity} = \frac{j}{S_{BET} * m} \quad \text{(S2)}$$

$$TOF = \frac{j\,N}{4F\Gamma} \quad \text{(S3)}$$

The term j, m and S_{BET} represent the current density at overpotential (η) of 350 mV, mass density at the electrode surface and BET surface of the synthesised OER catalyst respectively. N, F and Γare Avogadro's number, Faraday's constant and surface concentration of the catalyst.

The electrochemically available active sites of the materials were evaluated from the associated integrated charge of M^{2+} to M^{3+} redox reaction (Q) and e is the elementary charge (1.602×10^{-19} C). The equation is as follows:[2]

electrochemically available active sites = Q/e (S4)

For the post catalytic characterisations, at first catalyst ink was deposited on FTO coated glass substate (resistivity < 10 Ohms/sq) and then OER electrocatalysis was carried out. Finally, the material was collected from the FTO coated glass substrate for different characterisations.

Capacitance study:

Cyclic voltammogram were recorded using three electrode configurations in a potential range of -0.2 to 0.2 V vs Ag/AgCl (non-Faradaic region) at different scan rates (ν) to determine the areal capacitance, electrochemical active surface area (ECSA). The scan rates of the experiments were 50, 100, 200, 300, 400, 500, 600, 700 mV s-1. From CVs, the cathodic (i_c) and anodic (i_a) charging currents were determined at 0 V potential (vs Ag/ AgCl) at different scan rates (300, 400, 500, 600, 700 mV s-1) and the obtained current values were plotted against the scan rates. According to the Eqs S5 and S6 shown below the double layered capacitance (C_{dl}) of the catalyst was calculated from the average of two slopes in current vs. scan rate plots.[3] C_{dl} was divided by geometrical surface area (GSA) of the glassy carbon electrode to obtain the areal capacitance. ECSA was estimated by dividing C_{dl} with the specific capacitance (Cs = 27 μF cm^{-2})[3]

$$i_a = \nu C_{dl} \quad \text{(S5)}$$

$$i_c = \nu C_{dl} \quad \text{(S6)}$$

Mott−Schottky Analysis

Mott–Schottky measurements were carried out at frequency of 1000 Hz in the voltage range of −0.4 V to −1.4 V vs Ag/ AgCl with amplitude 0.005 V using three electrode configurations. In the Mott−Schottky theory, the space charge capacitance is dependant of on the potential, shown in the Eq S7:[4]

$$1/C_s^2 = 2/e\varepsilon\varepsilon_0 N_D\,(E_{applied} - E_{FB} - KT/e) \quad \text{(S7)}$$

where C_s represents the capacitance of the space charge region, e signifies the electronic charge (1.602×10^{-19} C), ε is the dielectric constant $(\varepsilon \sim 3.6)^2$, ε_0 being the vacuum permittivity given by 8.854×10^{-14} F cm^{-1}, $E_{applied}$ and E_{FB} are the applied and flat band potentials, N_D represents charge carrier density, k and T are the Boltzmann constant and absolute temperature at 298 K, respectively.

A linear fitting of $1/Cs^2$ versus V vs Ag/AgCl plot provides a slope which is equal to $2/q\varepsilon\varepsilon_0 N_D$. Using obtained slope from the plot a charge carrier concentration was determined from the relation, $N_D = 2/(q\varepsilon\varepsilon_0 \times \text{slope})$ for both the catalysts.

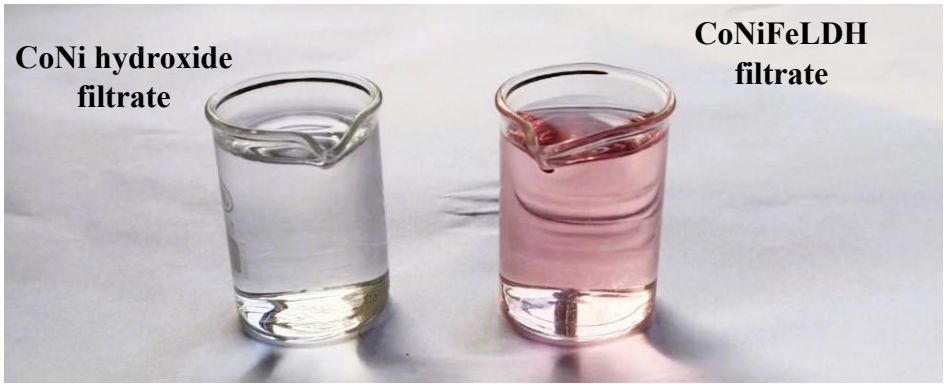

Fig. S1 The photograph of the collected filtrate at the initial stage of filtration.

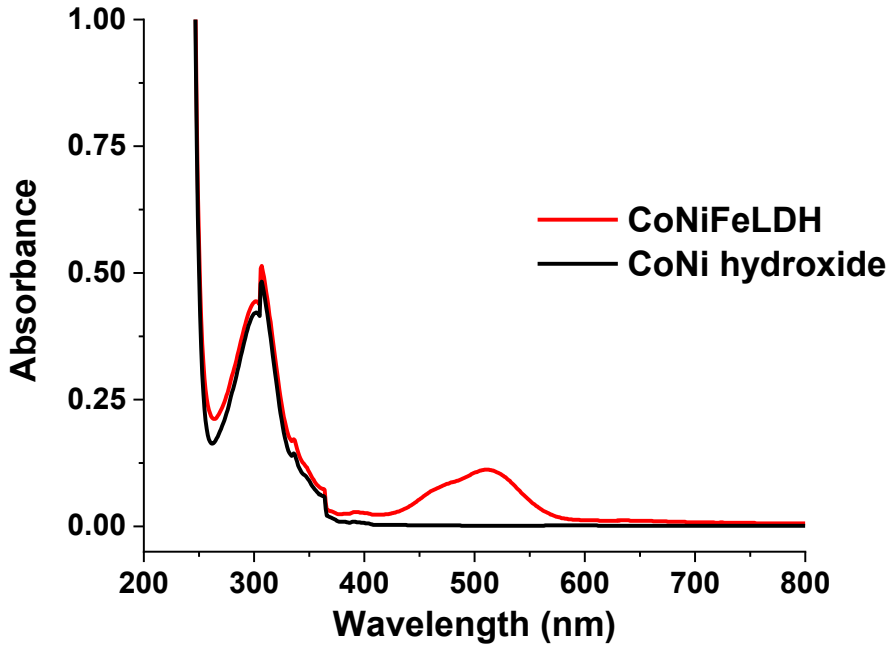

Fig. S2 UV-Vis spectra of filtrate of CoNi hydroxides and CoNiFeLDH at the initial stage of filtration.

ICP-OES SAMPLE ANALYSIS RESULTS

INSTRUMENT : PERKIN ELMER -AVIO 200

SAMPLE CODE : ASI-160

SL NO	SAMPLE NAME	Co (mg/l)	Ni (mg/l)	Fe (mg/l)
1	CN	650.9	244.4	----------

SL NO	ELEMENT NAME	Sample CNF (mg/l)
1	Co	296.800
2	Ni	152.700
3	Fe	636.200

Fig. S3 ICP-OES analysis for elemental analysis for CoNi hydroxides (CN) and CoNiFeLDH (CNF). A sample codes of CN and CNF were used for ICP-OES analysis.

Table S1 A comparison of Co:Ni in CoNi hydroxides and Co:Ni:Fe in CoNIFeLDH

Sample	Feeding ratio	ICP-OES analysis
CoNi hydroxide (CN)	Co: Ni=1.00:0.30	Co: Ni=1.00: 0.37
CoNiFe LDH (CNF)	Co: Ni: Fe= 1.00: 0.30:1.00	Co:Ni:Fe= 0.45: 0.23: 1.00

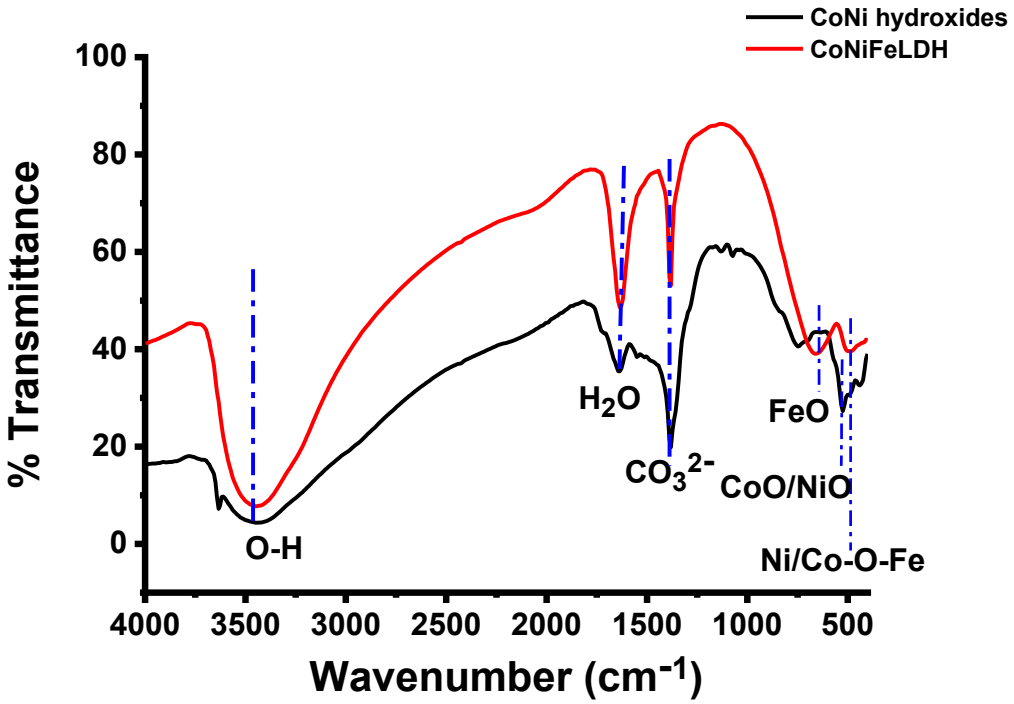

Fig. S4 FTIR spectra of CoNi hydroxides and CoNiFeLDH showing different bond vibrations of carbonates, water molecules and metal hydroxide.

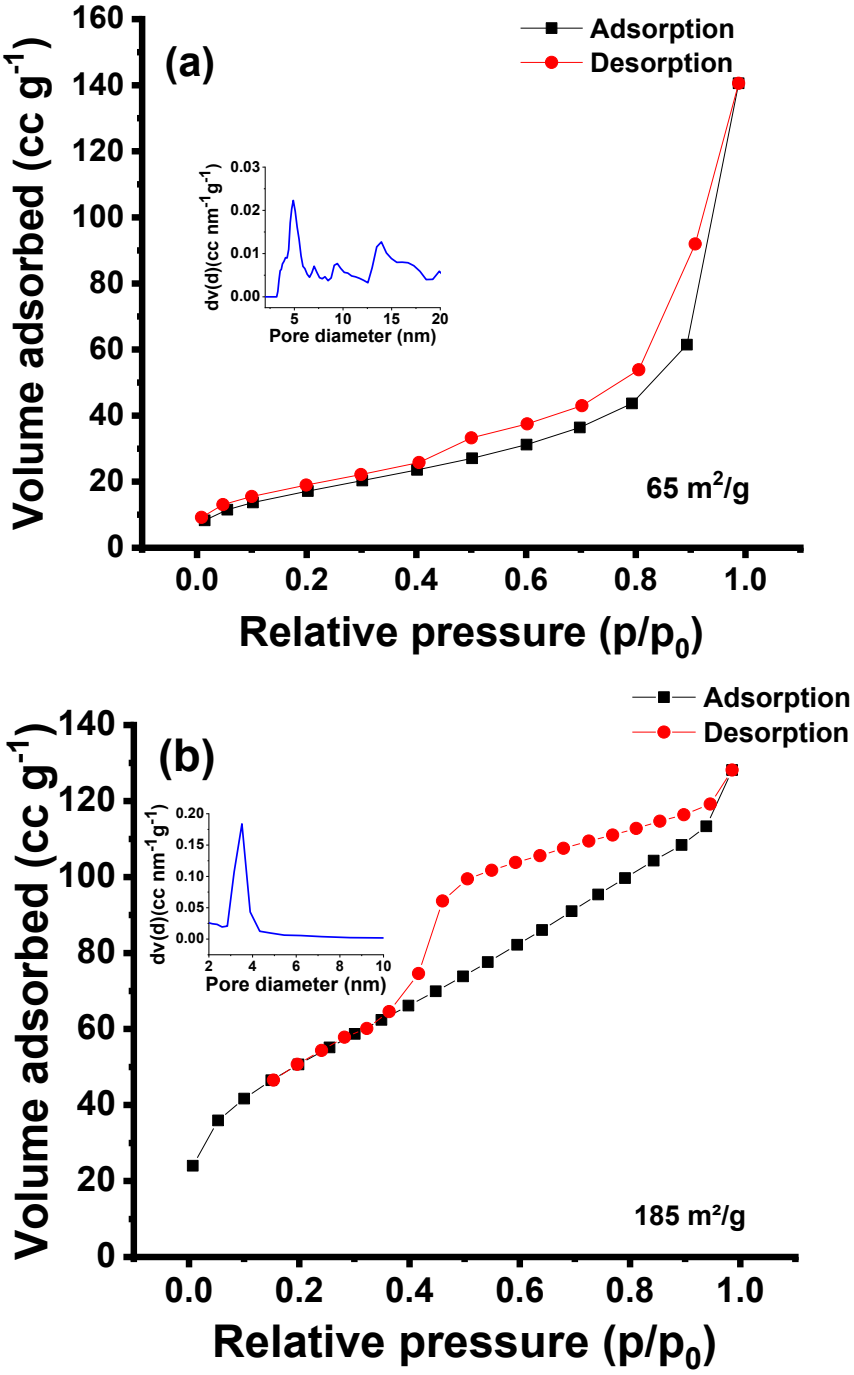

Fig. S5 N_2 adsorption - desorption isotherm and the pore size distribution (inset) of (a) CoNi hydroxides and (b) CoNiFeLDH. The surface area is provided for each case at right side of the respective figure.

Table S2 Comparison of the binding energy of the XPS peaks for Co, Ni, O in CoNi hydroxide and Co, Ni, Fe, O in CoNiFeLDH, with the reported earlier.[5,6]

Sample	Deconvoluted Co	Observed binding energy (eV)	Reported binding energy (eV)
CoNi hydroxide	Co^{3+} (2p3/2)	780.8	780.6
	Co^{2+} (2p3/2)	782.3	782.3
	Co^{3+} (2p1/2)	796.5	796.4
	Co^{2+} (2p1/2)	797.7	797.7
CoNiFeLDH	Co^{3+} (2p3/2)	780.7	780.6
	Co^{2+} (2p3/2)	782.2	782.3
	Co^{3+} (2p1/2)	796.5	796.4
	Co^{2+} (2p1/2)	797.7	797.7

Sample	Deconvoluted Ni	Observed binding energy (eV)	Reported binding energy (eV)
CoNi hydroxide	Ni^{2+} (2p3/2)	856.1	855.9
	Ni^{2+} (2p1/2)	873.6	873.4
CoNiFeLDH	Ni^{2+} (2p3/2)	856.2	855.9
	Ni^{2+} (2p1/2)	873.6	873.4

Sample	Deconvoluted Fe	Observed binding energy (eV)	Reported binding energy (eV)
CoNiFeLDH	Fe^{2+} (2p3/2)	711.2	711.0
	Fe^{3+} (2p3/2)	713.4	713.2
	Fe^{2+} (2p1/2)	725.4	724.5

Sample	Deconvoluted O	Observed binding energy (eV)	Reported binding energy (eV)
CoNi hydroxide	O1s (Lattice O)	530.8	529.5
	O1s (Adsorbed OH)	531.5	531.5
	Surface O-C=O	532.3	532.7
CoNiFeLDH	O1s (Lattice O)	531.1	529.5
	O1s (Adsorbed OH)	531.8	531.5
	Surface O-C=O	532.8	532.7

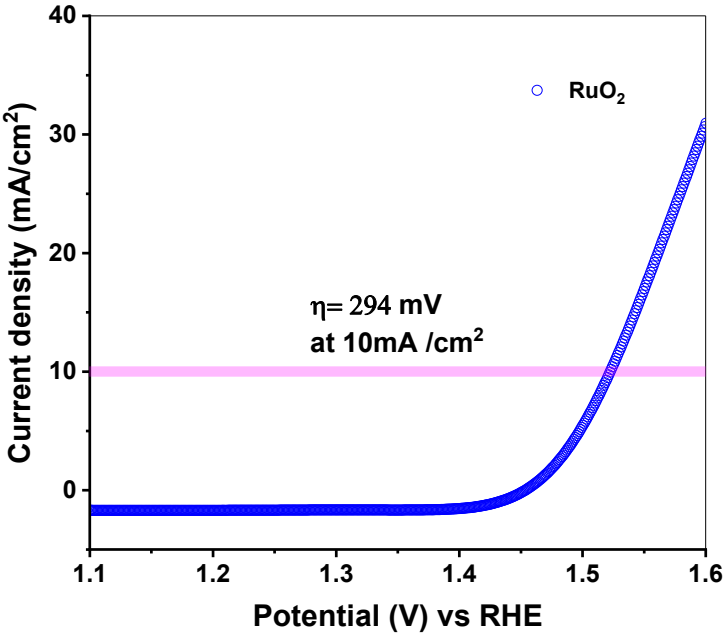

Fig. S6 Linear sweep voltammogram of RuO_2.

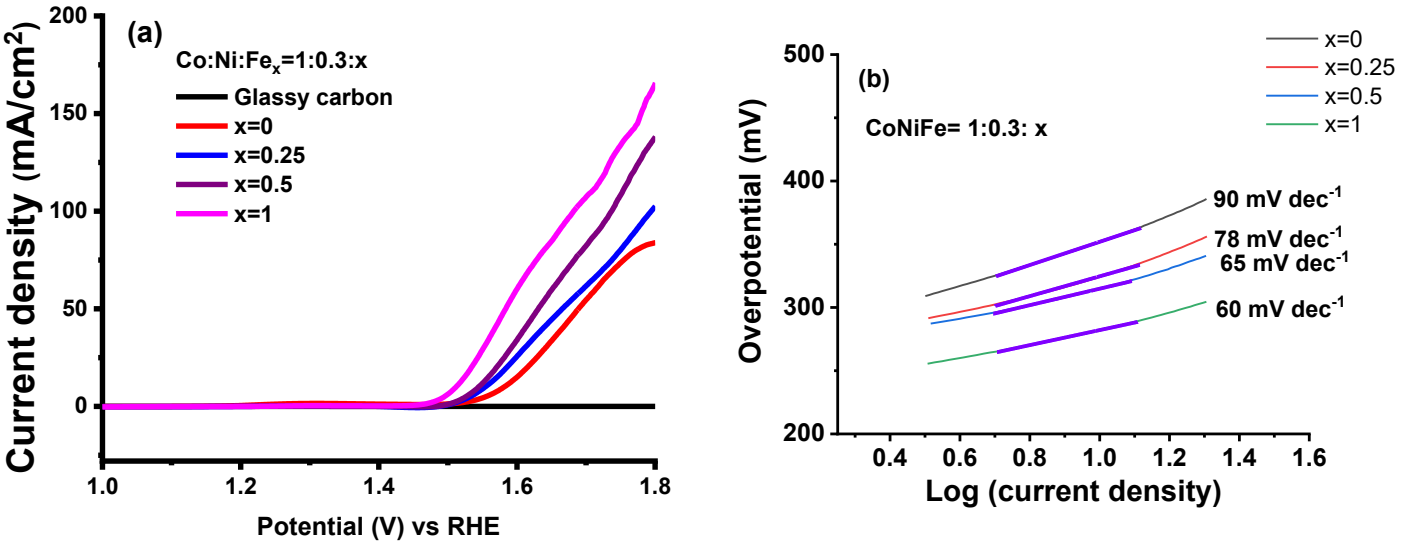

Fig. S7 (a) Linear sweep voltammograms and (b) Tafel plots of CoNiFex (x=0,0.25, 0.5, 1).

Table S3 Comparisons of overpotential, Tafe slope, TOF (s^{-1}), mass activity, specific activity of changed iron contents in the synthesis (x=0, 0.25, 0.5, 1).

Catalysts Co:Ni:Fe=1:0.3:x	Overpotential at 10 mA/cm^2	Tafel slope (mV dec^{-1})	TOF (s^{-1})	Mass activity@ η=350 mV (Ag^{-1})
x=0(CoNi hydroxide)	353 mV	90	0.17	148
x=0.25	324 mV	78	0.55	279
x=0.5	314 mV	65	1.85	377
x=1 (CoNiFeLDH)	280 mV	60	2.60	737

Determination of Turnover Frequency (TOF) from the Current Density of OER.[2]

Calculation of TOF for CoNi hydroxide: CoNiFex (x=0):

Current density: 9.68753 x 10^{-3} A/ cm^2 at 350 mV overpotential

Area under the curve associated with the of M^{3+} to M^{2+} from origin = 0.40472 x 10^{-3} AV/ cm^2

Total current: = 0.40472 x 10^{-3} A/ cm^2 x 0.07 cm^2 (electrode area)

= 0.00002813 AV

Associated charge= 0.00002813 AV/0.002 V s^{-1} (scan rate)

=0.0141 As

=0.0141 C

The number of electron transferred = 0.0141 C/ (1.602 x 10^{-19} C)

= 8.83 x 10^{16}

TOF at 350 mV overpotential: (9.68753 x 10^{-3}) x (6.022 x 10^{23})/ (96485 x 4 x 8.83 x 10^{16})

=0.17 s^{-1}

Calculation of TOF for CoNiFex (x=0.25)

Current density: 18.155 x 10^{-3} A/ cm^2 at 350 mV overpotential

Area under the curve associated with the of M^{3+} to M^{2+} from origin= 0.236 x 10^{-3} AV/ cm^2

Total current: = 0.236 x 10^{-3} A/ cm^2 x 0.07 cm^2 (electrode area)

= 0.00001652 AV

Associated charge= 0.00001652 AV/0.002 V s^{-1} (scan rate)

=0.00826 As

=0.00826 C

The number of electron transferred = 0.00826 C / (1.602 x 10^{-19} C)

= 5.15 x 10^{16}

TOF at 350 mV overpotential: (18.155 x 10^{-3}) x (6.022 x 10^{23})/ (96485 x 4 x 5.15x 10^{16})

=0.55 s^{-1}

Calculation of TOF for CoNiFex (x=0.5)

Current density: 24.53 x 10^{-3} A/ cm^2 at 350 mV overpotential

Area under the curve associated with the of M^{3+} to M^{2+} from origin= 0.0944 x 10^{-3} AV/ cm^2

Total current: = 0.0944 x 10^{-3} A/ cm^2 x 0.07 cm^2 (electrode area)

= 0.000006608 AV

Associated charge= 0.000006608 AV/0.002 V s^{-1} (scan rate)

=0.003304 As

=0.003304 C

The number of electron transferred = 0.003304 C / (1.602 x 10^{-19} C)

= 2.06 x 10^{16}

TOF at 350 mV overpotential: (24.53 x 10^{-3}) x (6.022 x 10^{23})/ (96485 x 4 x 2.06x 10^{16})

=1.85 s^{-1}

Calculation TOF for CoNiFeLDH: CoNiFex (x=1):

Current density: 48.1619 x 10^{-3} A/ cm^2 at 350 mV overpotential

Area under the curve associated with the of M^{3+} to M^{2+} from origin= 0.13214 x 10^{-3} AV/ cm^2

Total current: = 0.13214 x 10^{-3} A/ cm^2 x 0.07 cm^2 (electrode area)

= 0.0000092498 AV

Associated charge= 0.0000092498 AV/0.002 V s^{-1} (scan rate)

=0.004624 As

=0.004624 C

The number of electron transferred is = 0.004624C C/ (1.602 x 10^{-19} C)

= 2.886 x 10^{16}

TOF at 350 mV overpotential: (48.1619 x 10^{-3}) x (6.022 x 10^{23})/ (96485 x 4 x 2.886 x 10^{16})

=2.60 s^{-1}

Calculation of number of available active metal sites of CoNiFeLDH in OER[2]

Current density: 48.1619 x 10^{-3} A/ cm^2 at 350 mV overpotential

Area under the curve associated with the of M^{3+} to M^{2+} from origin= 0.13214 x 10^{-3} AV/ cm^2

Total current: = 0.13214 x 10^{-3} A/ cm^2 x 0.07 cm^2 (electrode area)

= 0.0000092498 AV

Associated charge= 0.0000092498 AV/0.002 V s^{-1} (scan rate)

=0.004624 As

=0.004624 C

The number of electron transferred is = 0.004624C C/ (1.602 x 10^{-19} C)

= 2.88 x 10^{16}

Since M^{3+} to M^{2+}change is a single electron transfer reaction, the number of electrons transferred in the process is equal to the number of available active metal sites.

Therefore, number of available active metal sites that involved in the OER electrocatalysis is

2.88 x 10^{16}

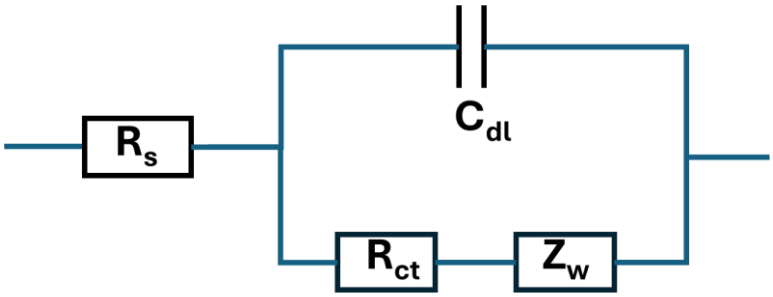

Fig. S8 Randel equivalent circuit; R_s: electrolyte resistance, C_{dl}: double layer capacitance, R_{ct}: charge transfer resistance and Z_w: Warburg impedance.

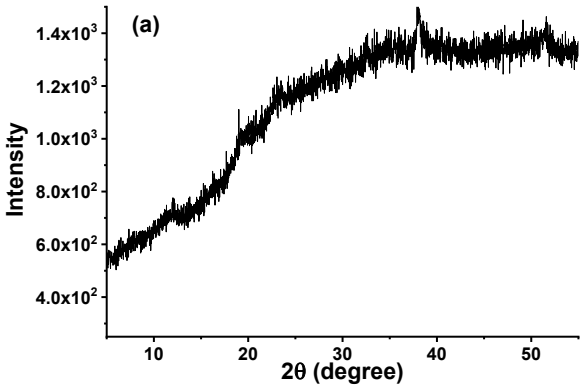

(b)

Label: CN #: 2
Analysis Type: UNKNOWN Analysis started at: 21/08/2025

Amount: Final Quantity: Standard DF: 1

Analyte (Measure Mode)	Concentration average
Ni 221.647 (Aqueous-Axial-iFR)	40.506 ppm
Co 237.862 (Aqueous-Axial-iFR)	136.818 ppm

Mole ratio of Co:Ni in CoNi hydroxide (CN) = 1.00:0.33

Fig. S9a,b XRD and ICP-OES analysis of CoNi hydroxide after OER electrocatalysis.

It was noticed that the semi crystalline characteristics and the quantitative Co and Ni mole ratio remained unaltered in ICP-OES after OER electrocatalysis. So, the possibility of structural mutation in this case was precluded. Therefore, the disintegration of the material from electrode surface became evident in the stability test. This has been reasonable in context of continuous oxygen bubbling in OER that brought mechanical stress to the material inducing disintegration and resulted in the decrease of OER activity.

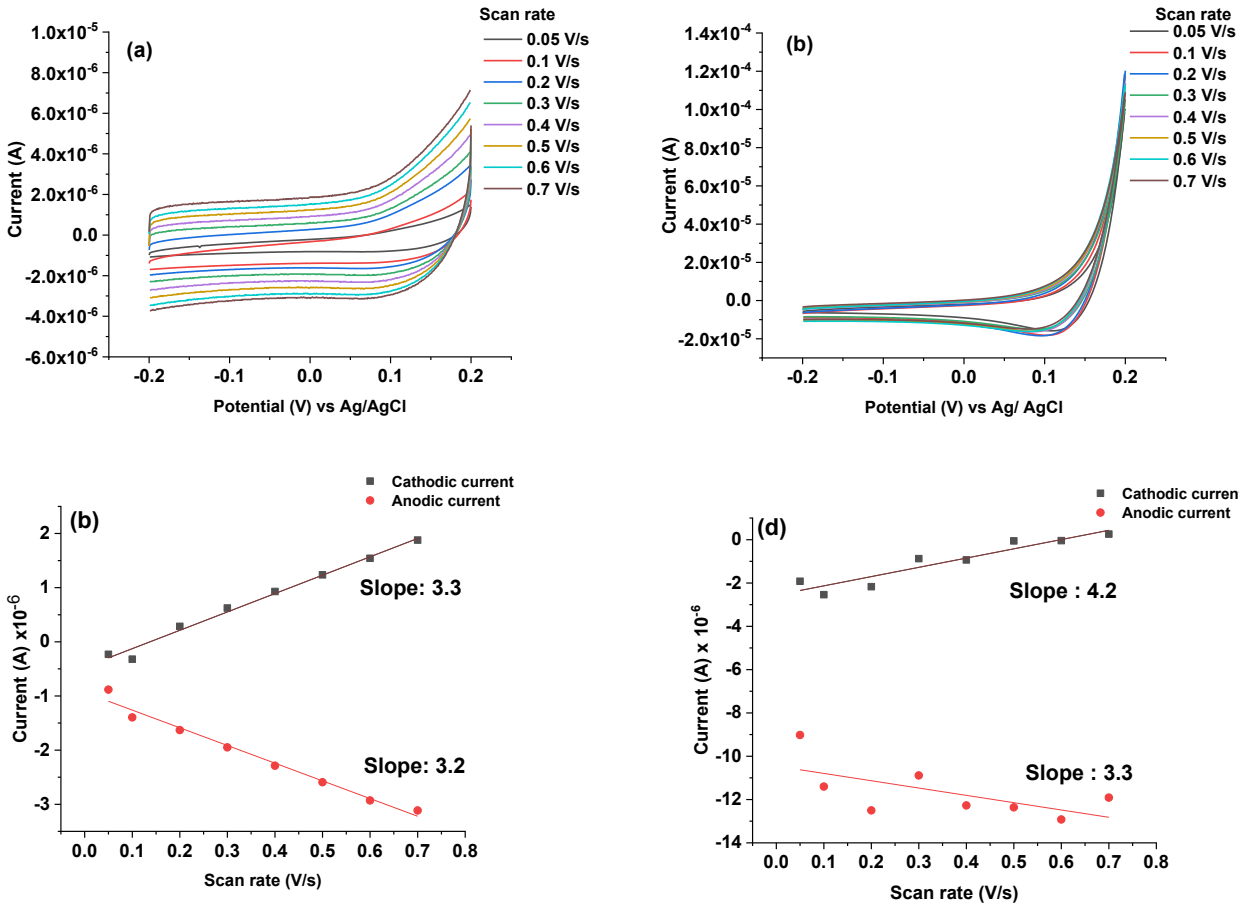

Fig. S10 Cyclic voltammograms of (a) CoNiFeLDH and (b) CoNi hydroxide recorded at different scan rates of 50, 100, 200, 300, 400, 500, 600, 700 mV s^{-1} (c,d) plots of cathodic and anodic currents at 0 V in different scan rates for CoNiFeLDH and CoNi hydroxide, respectively.

Table S4 Double layer capacitance, Areal capacitance, electrochemical active surface area, charge transfer resistance of the catalyst.

Catalyst	Double layer capacitance (C_{dl}, F)	Areal capacitance (F/cm^2)	ECSA (cm^2)	Charge transfer resistance (ohm)
CoNi hydroxide	3.82 x10^{-6}	54.65 x 10^{-6}	0.14	33
CoNiFeLDH	3.32 x10^{-6}	47.50 x 10^{-6}	0.12	17

Table S5 Comparisons of OER activity of Co, Ni, Fe based LDH catalysts with the reported earlier.

Sl No	Co, Ni and Fe based LDH electrocatalyst	Catalyst loading (mg cm^{-2})	η @10 mA cm^{-2} (mV)	Tafel slope (mV dec^{-1})	Ref.
1.	*CoNiFeLDH*	*0.06*	*280*	*60*	*Our work*
2.	NiFe LDH nanosheets anchored on cobalt nanocrystal	0.4	282	64	*ACS Appl.NanoMater.,*2022, **5**, 13047
3.	Co-Ni-Fe LDH	0.14	322	41.8	*J. Colloid Interface Sci.,* 2025, **678**, 924
4.	Ni-Co-Fe hydr(oxy)oxide@Ni-Co LDH	0.33	278	49.7	*Angew. Chem. Int. Ed.* 2022, **61**, e202213049
5.	Trimetallic NiCoFe-LDH	2.8	277	68.8	*ACS Sustain. Chem. Eng.* 2022, **10**, 14693
6.	FeCoNi LDH	0.25	269	42.3	*Adv. Energy Mater.* 2021, **23**, 2102141
7.	NiCoFe-LDH nanosheets	18.8	288	92	*ACS Catal.,* 2020, **10**, 5179
8.	Ternary NiCoFe-LDH hollow polyhedrons	1.0	276	56	*J. Energy Chem.* 2020, **43**, 104
9.	NiCoFe-LDH/N-doped graphene oxide	0.28	317	56.8	*Adv. Energy Mater.* 2017, **8**, 1701905
10	CoNiFe LDH/GC	0.20	291	59	*ACS Appl. Energy Mater., 2018,* **1**, *4998*
11	*CoNiFe subacetate nanoprism*	0.4	292	75.6	*New J. Chem. 2023,* **47**, *18532*
12.	*CoCuFe LDH/graphene*	0.25	350	62.6	*ACS Appl. Mater. Interfaces,* 2024, **16**, 50846

Comparison of turn over frequency (TOF) and mass activity:

	LDH Catalyst	TOF (s^{-1})	Mass activity (Ag^{-1})	Electrolyte	Ref.
1.	*CoNiFeLDH*	*2.6 @350 mV*	*730 @350 mV*	*1M KOH*	*Our work*
2.	CoFe-LDH	4.22 @300 mV	559.2 @350 mV	1M KOH	*ACS Appl. Nano Mater.,* 2024, **7**, 9532
3.	NiFeLDH/OC	1.05 @300 mV	528 @350 mV	1M KOH	*Chem. Commun*. 2020, **56**, 8770
4.	Co_3Fe_1LDH/rGO/NF	6.0 * 10^{-2} @ 300 mV	26.02 @ 400 mV	1M KOH	*Int. J. Hydrog. Energy.,* 2021, **46**, 27529
5.	$Co_{0.4}Fe_{0.6}$ LDH/g-CN_x	2.5 * 10^{-1} @ 350 mV	1353 @ 340 mV	1 M KOH	*ACS Appl. Energy Mater.,* 2018, **1**, 1200

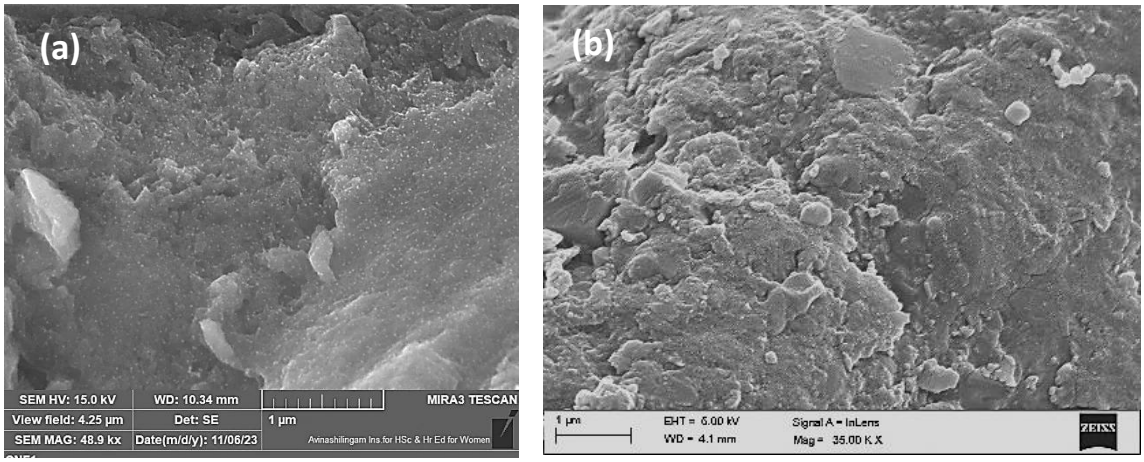

Fig. S11 SEM analysis of CoNiFeLDH (a) before and (b) after electrocatalysis.

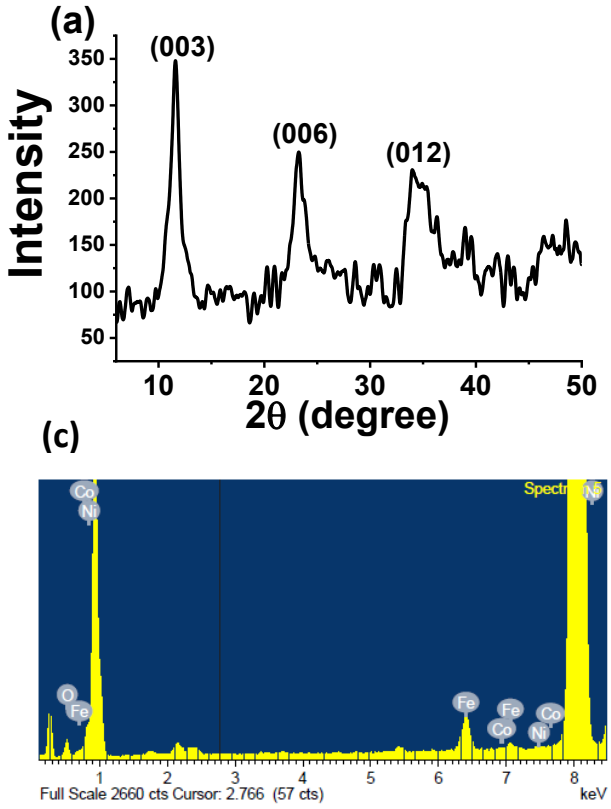

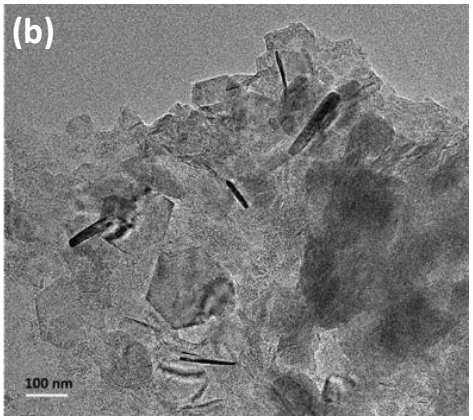

(d)

Label: CNF #: 1
Analysis Type: UNKNOWN Analysis started at: 21/08/2025

Amount: Final Quantity: Standard DF: 1

Analyte (Measure Mode)	Concentration average
Ni 221.647 (Aqueous-Axial-iFR)	54.095 ppm
Co 237.862 (Aqueous-Axial-iFR)	125.536 ppm
Fe 259.837 (Aqueous-Axial-iFR)	151.700 ppm

Mole ratio of Co:Ni:Fe in CoNiFeLDH (CNF) = 0.78:0.33:1.00

Fig. S12 (a) XRD, (b, c) HRTEM, EDS and (d) ICP-OES of CoNiFeLDH after electrocatalysis.

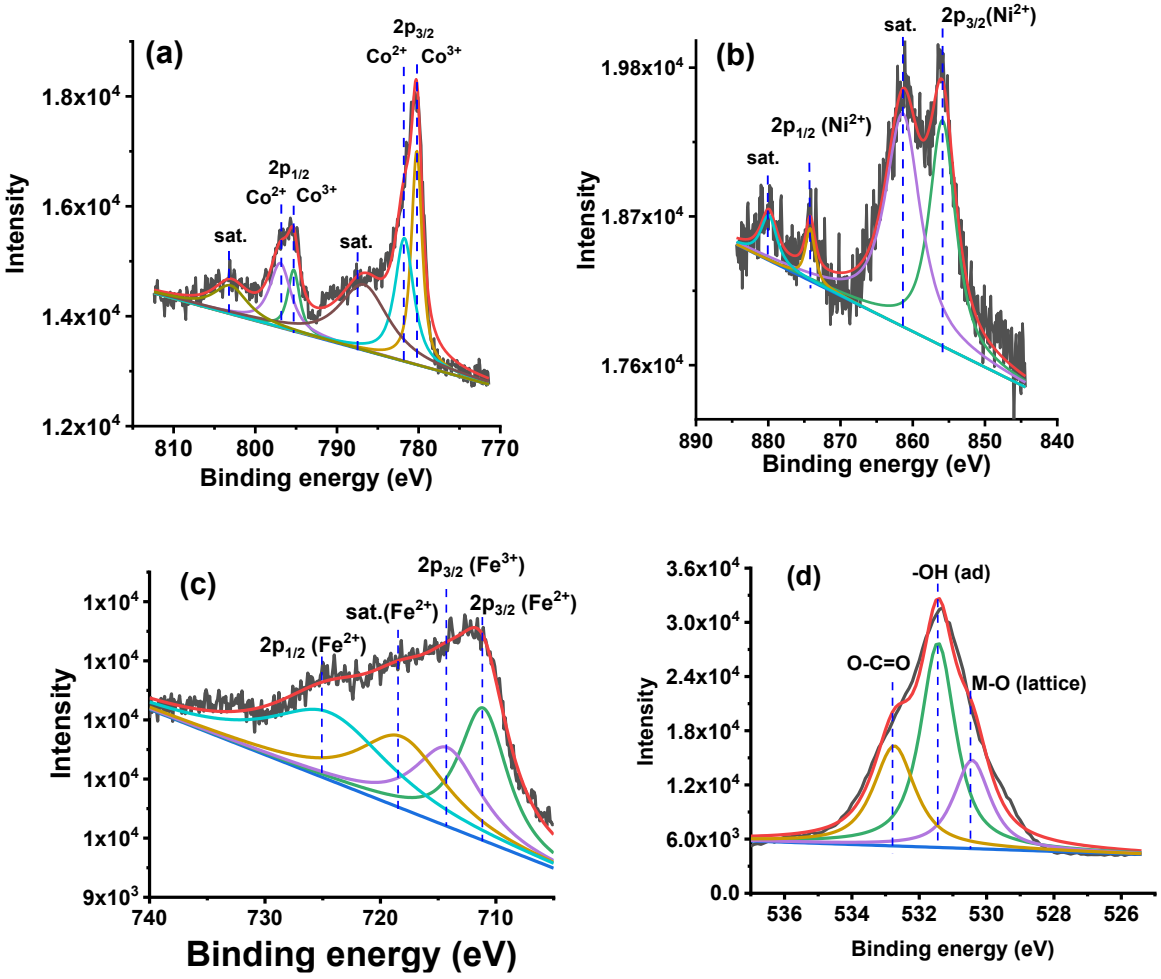

Fig. S13 High resolution XPS spectra of (a) Co_{2p}, (b) Ni_{2p}, (c) Fe_{2p} and (d) O_{1s} of CoNiFeLDH after electrocatalysis.

Table S6 Binding energy of the XPS peaks for Co, Ni, O in CoNiFeLDH after electrocatalysis compared with the reported earlier.[5,6.]

Sample	Deconvoluted Co	Observed binding energy (eV) before OER (Table S2)	Observed binding energy (eV) post OER	Reported binding energy (eV)
CoNiFeLDH	Co^{3+} (2p3/2)	780.7	780.2	780.6
	Co^{2+} (2p3/2)	782.2	781.9	782.3
	Co^{3+} (2p1/2)	796.5	795.5	796.4
	Co^{2+} (2p1/2)	797.7	797.0	797.7

Sample	Deconvoluted Ni	Observed binding energy (eV) before OER (Table S2)	Observed binding energy (eV) post OER	Reported binding energy (eV)
CoNiFeLDH	Ni^{2+} (2p3/2)	856.2	856.0	855.9
	Ni^{2+} (2p1/2)	873.6	874.1	873.4

Sample	Deconvoluted Fe	Observed binding energy (eV) before OER (Table S2)	Observed binding energy (eV) post OER	Reported binding energy (eV)
CoNiFeLDH	Fe^{2+} (2p3/2)	711.2	711.1	711.0
	Fe^{3+} (2p3/2)	713.4	714.2	713.2
	Fe^{2+} (2p1/2)	725.4	725.0	724.5

Sample	Deconvoluted O	Observed binding energy (eV) before OER (Table S2)	Observed binding energy (eV) post OER	Reported binding energy (eV)
CoNiFeLDH	O1s (Lattice O)	531.1	530.4	529.5
	O1s (Adsorbed OH)	531.8	531.5	531.5
	Surface O-C=O	532.8	532.8	532.7

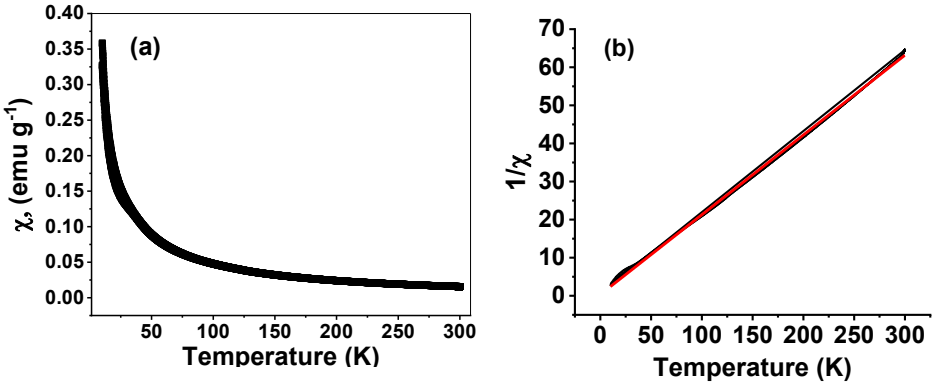

Fig. S14 (a) Zero-field-cooling (ZFC) temperature-dependent magnetic susceptibility of CoNiFeLDH and (b) A plot of 1/χ vs. T to determine inverse magnetic susceptibility. The red solid line is a fit to the susceptibility data to the Curie–Weiss law.

Calculation of magnetic moment and number of unpaired electrons to determine spin state:[7]

A linear fitting of 1/χ vs. T in Fig. S14 enabled to obtain the slope as 1/ C following the Curie–Weiss equation as:

$\chi^{-1}=(T-\theta_{CW})/C = T/C-\theta_{CW}/C$

where χ, C and θ_{CW} are the magnetic susceptibility, Curie constant and Curie–Weiss temperature, respectively.

Using C (Curie constant) the effective magnetic moment in $\mu_{eff} = \sqrt{(8C)}\ \mu_B$, can be determined and following number of unpaired electrons were found by $\mu_{eff} = \sqrt{n(n+2)}\ \mu_B$ where n is number of unpaired electrons and μ_B is Bohr magneton.

From the slope of the linear fitting in Fig X was found to be C is 4.76 emu K g^{-1}

Applying $\mu_{eff} = \sqrt{(8C)}\ \mu_B$,

$\mu_{eff} = 6.17\ \mu_B$

$\mu_{eff} = \sqrt{[n(n+2)]}\ \mu_B$

$(6.17)^2 = n(n+2)$

$38.07 = n^2 + 2n$

Rearrange the equation into a quadratic form:

$n^2 + 2n - 38.07 = 0$

Solve for n using the quadratic formula

$n = [-b \pm \sqrt{(b^2 - 4ac)}] / 2a$

In this case, a = 1, b = 2, and c = -38.07.

$n = [-2 \pm \sqrt{(2^2 - 4 \times 1 \times -38.07)}] / (2 \times 1)$

$n = [-2 \pm \sqrt{(4 + 152.28)}] / 2$

$n = [-2 \pm \sqrt{(156.28)}] / 2$

$n = [-2 \pm 12.50] / 2$

Calculate the two possible values for n: $n_1 = (-2 + 12.50) / 2 = 10.50 / 2 = 5.25$

$n_2 = (-2 - 12.50) / 2 = -14.50 / 2 = -7.25$

Therefore, an effective magnetic moment of 6.17 μ_B corresponds to approximately 5 unpaired electrons and hence proved that Fe^{3+} is present in high spin (t_{2g}^3 e_g^2).

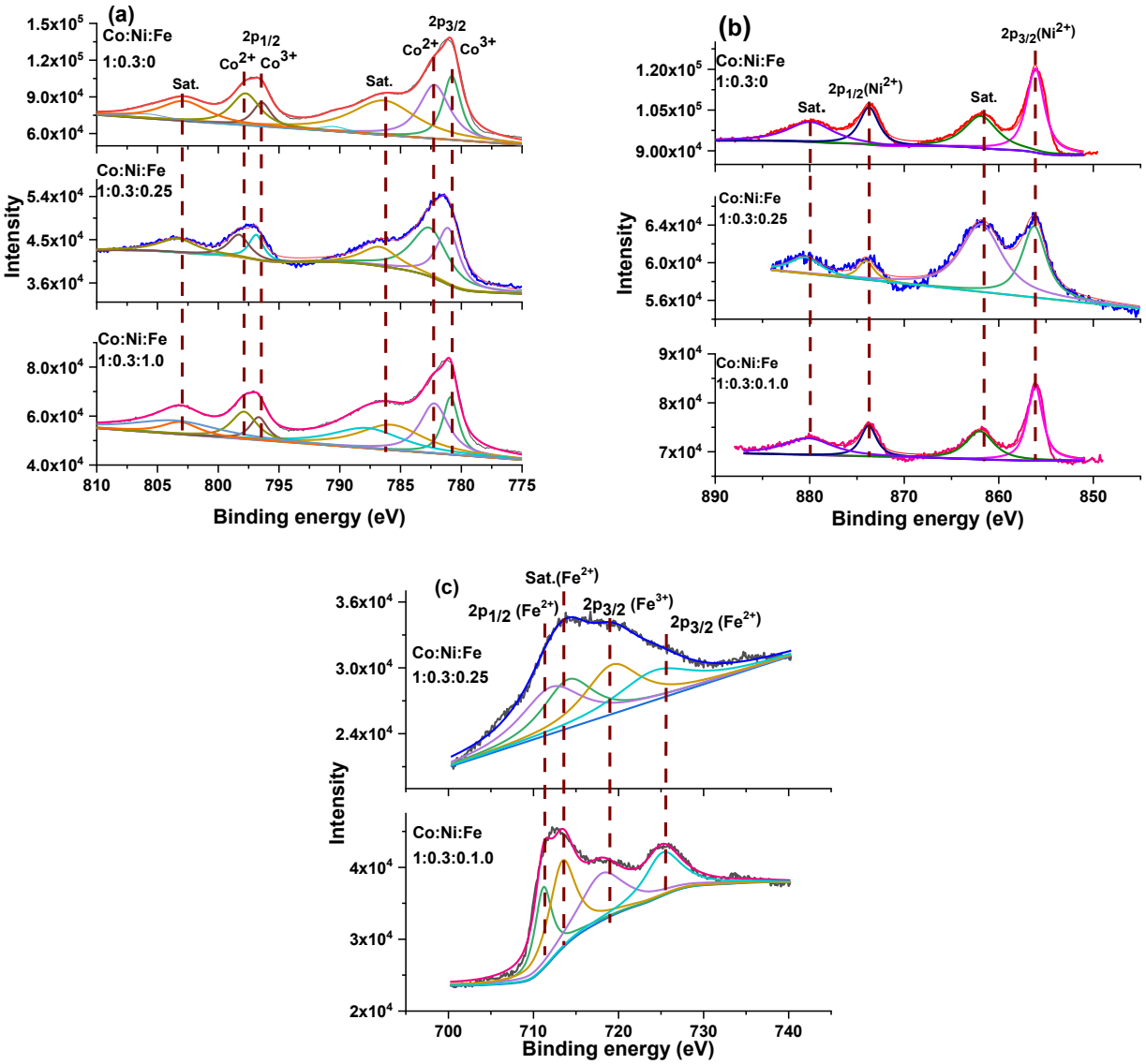

Fig. S15 High resolution XPS analysis of (a) Co_{2p}, (b) Ni_{2p} and (c) Fe_{2p} of CoNiFex (x=0, 0.25, 1) varying iron concentration.

Discussion on the change transfer in CoNiFeLDH during OER.

It has been already found that oxidation states of Co ($Co^{2+,}$ Co^{3+}) and Ni (Ni^{2+}) was identical for Co:Ni:Fe = 1.00:0.30:0.00 (CoNi hydroxide) and Co:Ni:Fe = 1.00:0.30:1.00 (CoNiFeLDH). We carried out another XPS analysis of Co:Ni:Fe = 1.00:0.30:0.25 to compare the oxidation state of metal ions varying iron contents in Fig. S15and explore the impact of the low concentration of Fe (Fe=0.25) in the metal hydroxide. The high resolution XPS of Co($2p_{1/2}$, $2p_{3/2}$) in Co:Ni:Fe = 1.00:0.30:0.25 showed small shift towards higher binding energy of 0.3 eV compared to other two compositions, this can be due to local change in electronic environments around metal centre for inclusion of Fe. However, the XPS scan for Ni_{2p} and Fe_{2p} were identical for three compositions (CoNiFex (x=0, 0.25, 1)). Comparing the XPS analysis of all three materials, it can be unveiled that that added iron in the material has insignificant role to alter oxidation of other co-existing metal centers in the synthesis stage. Hence, the XPS experiment also supports the concept of redox chemistry where it is known that varying iron contents in same oxidation states in metal hydroxides was not effective to the change the

oxidation states of the co-existing metal ions except the minor change in the electronic properties of metal centers around it. It is to be noted that the importance of the facile charge transfer in Fe-O-Ni and Fe-O-Co units due to the suitable oxidation states of the metal ions of CoNiFeLDH (Fig. 6) in the context of OER was already proposed. Accordingly, the crystal field theory with a schematic and the evidence from the literature reports were used to explain the enhanced OER kinetics.[4,8,9] Simultaneously, it has been seen that OER activity was gradually improved with increased concentration of Fe from CoNi hydroxide to CoNiFeLDH in Fig. S6. Therefore, the enhanced OER activity can be rationalized by the greater number of the charge transfer possibilities with the increased iron concentration when the material is present at the electrode-electrolyte interface under the influence of oxidation potential in OER.

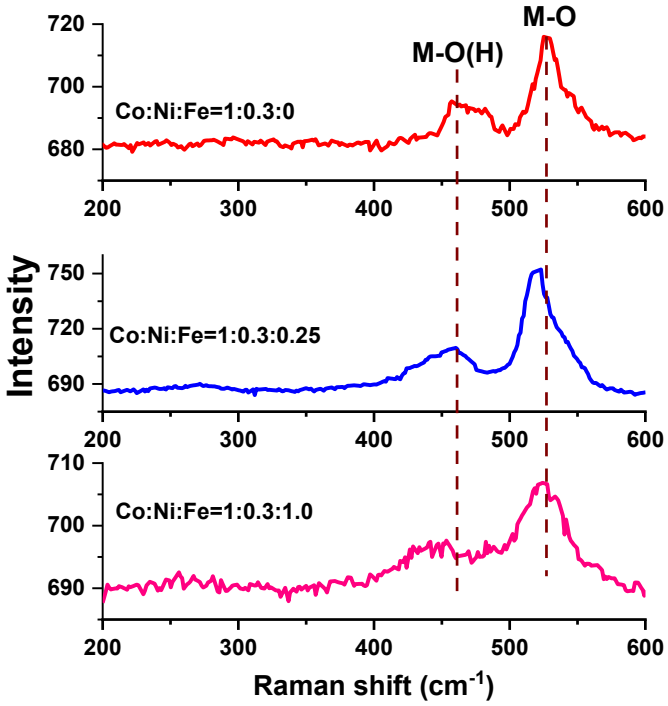

Fig. S16 Raman analysis for CoNiFex (x=0, 0.25, 1) varying iron concentration.

Raman analysis has been carried for all three compositions of different iron contents for Co:Ni:Fe =1.00 :0.30:0.00, Co:Ni:Fe =1.00:0.30:0.25 and Co:Ni:Fe =1.00:0.30: 1.00. We witnessed the shifting of peak position of M-O bond to lower wave number on increasing the Fe concentration from Co:Ni:Fe =1.00 :0.30:0.00 (CoNi hydroxide) to Co:Ni:Fex (x=0.25, 1) although there was no significant shift observed between the Fe containing metal hydroxides. The shifting was found to be from 527 cm^{-1} to 520 ±1 cm^{-1}.[10] This is due to the phonon softening arising from the tensile strain developed in metal hydroxides with the added Fe^{3+} of smaller ionic radii compared to Co^{2+} and Ni^{2+} ions. It resulted in the elongation M-O bonds. In addition, the appearance of the broad peak around 458 cm^{-1} indicated the existence of the defects of all metal hydroxides.[11] The broadness is most prominent in case of highest iron content among three samples which is evident for lattice strain that also supported the evolution of LDH in the x-ray diffraction analysis. The lattice strain could make additional contribution for enhanced OER due to efficient adsorption of oxygenated intermediate as evidenced by Liu et al.[12]

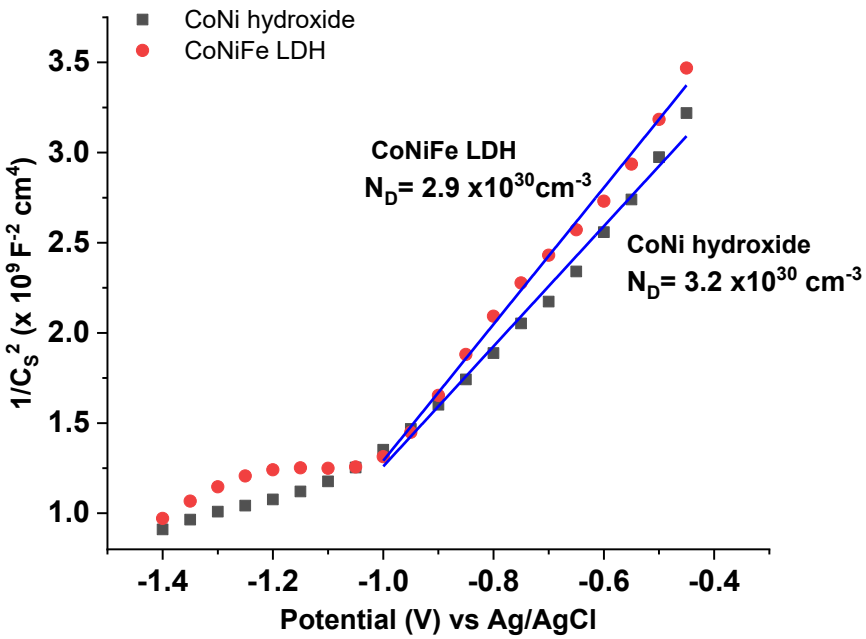

Fig. S17 Mott–Schottky plots of CoNi hydroxide and CoNiFe LDH.

Calculation of charge carrier density (N_D) from Mott–Schottky plots

$N_D = 2/ (q\varepsilon\varepsilon 0 \times \text{slope})$

Where q indicates the electronic charge (1.602×10^{-19} C), ε being the dielectric constant ($\varepsilon \sim 3.6$)^2, ε0 is the vacuum permittivity (8.854×10^{-14} F cm^{-1}) and the slope is obtained from $1/Cs^2$ vs potential (V) vs /Ag/AgCl plots.

N_D (CoNi hydroxide) = $2/ (1.602 \times 10^{-19}$ C x $(3.6)^2$ x 8.854×10^{-14} x 3.3)

$=3.20 \times 10^{30}$ cm^{-3}

N_D (CoNiFe LDH) = $2/ (1.602 \times 10^{-19}$ C x $(3.6)^2$ x 8.854×10^{-14} x 3.7)

$=2.90 \times 10^{30}$ cm^{-3}

Table S7 Comparisons of the different synthetic protocols of Co, Ni and Fe based LDH catalysts with the previous reports.

Sl	Trimetallic LDH	Synthesis process	Synthesis temperature	Synthesis time	Ref.
1.	*CoNiFeLDH*	*Coprecipitation*	*Room temperature*	*24 h*	*Our work*
2.	NiCoFe-LDH Nanosheets	Hydrothermal	100 ^{O}C	Overnight	*ACS Catal*., 2020, **10**, 5179
3.	NiCoFe-LDH/N-Doped Graphene Oxide	Coprecipitation	Room temperature	24 h	*Adv. Energy Mater.,* 2017, **8** 1701905
4.	Ternary NiFeCo metal compound	Corrosion reaction using Ni foam	90 ^{O}C	12 h	*Appl. Catal. B,* 2021, **294**, 120246
5.	Defect-Rich Ternary NiCoFe LDH	Electrodeposition On Ni foam	Room temperature	-	*Chem. Eur. J*, 2022, **28**, e202103601
6.	Cobalt-promoted formation of oxygen vacancy in NiFe LDH	Hydrothermal	120 ^{O}C	24 h	*J. Power Sources,* 2021, **506**, 230097
7.	Superhydrophilic cobalt-doped NiFe LDH	Hydrothermal	120 ^{O}C	12 h	*Int. J. Hydrog. Energy,* 2024, **80**, 11
8.	Co3S4@NiFe-LDH	Electrodeposition On Co_3S_4 nanosheet	Room temperature	200s	*ACS Appl. Mater. Interfaces,* 2024, **16**, 8751
9.	Layered NiFeCo Double Hydroxide Nanosheets	Hydrothermal	120 ^{O}C	12 h	*ACS Appl. Nano Mater.* 2024, **7**, 13308
10.	NiCoFe-layered hydroxide grown on graphene oxide	(i) coprecipitation (ii hydrothermal	(i) 60 ^{O}C (ii) 120 ^{O}C	(i) 30 min (ii)24 h	*New J. Chem.,* 2024, **48**, 10739
11.	An amorphous trimetallic (Ni–Co–Fe) hydroxide	Hydrothermal	180 ^{O}C	6h	*J. Mater. Chem. A*, 2020, **8**, 5601
12.	NiFe LDH Nanosheets Anchored on Cobalt Nanocrystal	Hydrothermal	100 ^{O}C	6h	*ACS Appl.NanoMater.,* 2022, **5**, 13047
13.	NiFeCo LDHQDs-modified NiCoP nanoarray	(i)Hydrothermal (ii)coprecipitation	(i) 120 ^{O}C (ii) 80 ^{O}C	8h -	*Inorg. Chem. Front*., 2024, **11**, 4794
14.	NiFeCo-LDH nanosheets supercapacitor	Hydrothermal	160 ^{O}C	4h	*J. Mater. Chem. A,* 2024, **12**, 2887
15.	NiCoFeLDH	hydrothermal	95 ^{O}C	8h	*Int. J. Hydrog. Energy,* 2022, **47**, 23644
16.	Ternary NiCoFe-LDH hollow polyhedrons	Templating with metal-organic framework (ZIF-67)	Room temperature	1h	*J. Energy Chem*., 2020, **43**, 104
17.	Hierarchical trimetallic LDH nanosheets	Templating with metal-organic framework	Room temperature	10 min	*Appl. Catal. B,* 2020, **264**, 118532
18.	FeCoNi LDH	Templating with metal-organic framework (ZIF-67)	Room temperature	6h	*Adv. Energy Mater.,* 2021 **23**, 2102141
19.	Metal–Organic Framework-Derived Trimetallic NiCoFe-LDH	Templating with metal-organic framework	Ambient temperature	6h	*ACS SustainableChem.Eng.*2022, **10**, 14693
20.	Ni-Co-Fe Hydr(oxy)oxide@Ni-Co LDH	Templating with metal-organic framework (ZIF-67)	92 ^{O}C	15 min	*Angew. Chem. Int. Ed.,* 2022, **61**, e202213049

References:

1. M. Gao, W. Sheng, Z. Zhuang, Q. Fang, S. Gu, J. Jiang and Y. Yan, *J. Am. Chem. Soc*. 2014, **136**, 7077-7084.

2. S. Roy, R. Madhu, K. Bera, S. Nagappan, H. Dhandapani, A. De and S. Kundu, *ACS Appl. Mater. Interfaces*, 2024, **16**, 5965–5976.

3. C. McCrory, S. Jung, I. Ferrer, S. Chatman, J. Peters and T. Jaramillo, *J. Am. Chem. Soc*. 2015, **137**, 4347–4357.

4. S. Deka, M. Jaiswal, P. Rajput and B. Choudhury, *J. Mater. Chem. A*, 2024, **12**, 9532–9545.

5. J. Song, B. Zhao, Y. Huang, Y. Qin, J. Zhou, W. Song and Y. Sun, *RSC Adv*., 2017, **7**, 2745–2752.

6. A. Bovas and T. Radhakrishnan, *J. Mater. Chem. A*, 2024, **12**, 24872- 24877.

7. X. Xua and J. Guan, *Chem. Sci*., 2024, **15**, 14585 -14607.

8. M. Liu, K. Min, B. Han and L. Lee, *Adv. Energy Mater*., 2021, **11**, 2101281.

9. J. Jiang, F. Sun, S. Zhou, W. Hu, H. Zhang, J. Dong, Z. Jiang, J. Zhao, J. Li, W. Yan and M. Wang, *Nat. Commun*., 2018, **9**, 2885.

10. S. Liu, Y. Zhang, L. Hao, A. Nsabimana, S. Shen, *J. Colloid Interface Sci*., 2025, **678**, 924–933.

11. B. Lee, S. Jung, G. Yu, H. Kim, J. Kwon, K. Kim, J. Kwak, W. Lee, D. Mok, S. Back and Y. Kim, *ACS Catal*., 2025, **15**, 1123−1134.

12. D. Zhou, S. Wang, Y. Jia, X. Xiong, H. Yang, S. Liu, J. Tang, J. Zhang, D. Liu, L. Zheng, Y. Kuang, X. Sun and B. Liu, *Angew. Chem. Int. Ed.*, 2019, **58**, 736−740.